



CHORUS

This is the accepted manuscript made available via CHORUS. The article has been published as:

Phonon anomalies in pyrochlore iridates studied by Raman spectroscopy

K. Ueda, R. Kaneko, A. Subedi, M. Minola, B. J. Kim, J. Fujioka, Y. Tokura, and B. Keimer
Phys. Rev. B **100**, 115157 — Published 27 September 2019

DOI: [10.1103/PhysRevB.100.115157](https://doi.org/10.1103/PhysRevB.100.115157)

Phonon anomalies in pyrochlore iridates studied by Raman spectroscopy

K. Ueda,¹ R. Kaneko,² A. Subedi,³ M. Minola,¹ B. J. Kim,^{1,4,5} J. Fujioka,^{6,7} Y. Tokura,^{2,8} and B. Keimer¹

¹*Max-Planck-Institut für Festkörperforschung, Heisenbergstr. 1, D-70569 Stuttgart, Germany*

²*Department of Applied Physics, University of Tokyo, Tokyo 113-8656, Japan*

³*Centre de Physique Théorique, Ecole Polytechnique, CNRS, France*

⁴*Department of Physics, Pohang University of Science and Technology, Pohang 790-784, Republic of Korea*

⁵*Center for Artificial Low Dimensional Electronic Systems,*

Institute for Basic Science (IBS), Republic of Korea

⁶*PRESTO, Japan Science and Technology Agency, Kawaguchi, Saitama 332-0012, Japan*

⁷*University of Tsukuba, 1-1-1 Tennodai, Tsukuba, Ibaraki, 305-8573, Japan*

⁸*Center for Emergent Matter Science (CEMS), RIKEN Advanced Science Institute (ASI), Wako 351-0198, Japan*

(Dated: September 9, 2019)

We report polarization-resolved Raman scattering measurements on single crystals of the pyrochlore compound $\text{Eu}_2\text{Ir}_2\text{O}_7$ which exhibits a ground state with non-collinear magnetic order, as well as its paramagnetic counterpart $\text{Pr}_2\text{Ir}_2\text{O}_7$. The spectra reveal the six Raman-active optical phonons expected for the pyrochlore lattice symmetry. Combined with density functional calculations, polarization analysis of the Raman intensity allows us to assign all observed peaks to specific vibration patterns. Whereas most phonon profiles are weakly temperature dependent, an Ir-O-Ir bond-bending vibration in $\text{Eu}_2\text{Ir}_2\text{O}_7$ exhibits a pronounced Fano asymmetry in the paramagnetic state, and marked softening and lineshape anomalies at the magnetic phase transition. These observations indicate strong electron-phonon interactions, which must be considered in models of the electronic properties and phase behavior of the pyrochlore iridates. In addition, a prominent feature appears at 210 cm^{-1} in the Raman spectrum of $\text{Eu}_2\text{Ir}_2\text{O}_7$ below the magnetic transition temperature, possibly due to a magnetic excitation.

Electronic correlations and topological phenomena are major themes of contemporary solid-state physics. Whereas research in both areas evolved from different origins, several emerging research frontiers now encompass both strong electronic correlations and topological complexity; prominent examples include topological superconductors and Kitaev spin liquids.¹ Materials with $4d$ - and $5d$ -electrons are fertile platforms for exploration of these ideas, because the large spin-orbit coupling (SOC) of the valence electrons can both effectively enhance electronic correlations (by narrowing the valence band)² and generate topologically complex wavefunctions (by promoting spin-momentum locking).³

Iridates of composition $R_2\text{Ir}_2\text{O}_7$ (where R is a rare earth element) have received particular recent attention in this regard. The Ir^{4+} ions with valence electron configuration $5d^5$ and total angular momentum $J = \frac{1}{2}$ are arranged on the geometrically frustrated pyrochlore structure. Due to the confluence of strong SOC, strong Coulomb correlations, and geometric frustration, the pyrochlore iridates undergo multiple magnetic and metal-insulator transitions as a function of temperature, chemical composition⁴⁻⁶, pressure⁷⁻⁹, and magnetic field¹⁰⁻¹³. Figure 1 shows the phase diagram as a function of temperature and the radius of the R ions, which modulates the valence-electron bandwidth and hence the effective correlation strength. Whereas compounds with large R and large bandwidth are paramagnetic metals in the entire temperature range^{14,15}, compounds with smaller R exhibit a magnetically ordered state with sharply reduced electrical conductivity below a temperature T_N that depends on R . The magnetic ordering

pattern is the so-called “all-in/all-out” (AIAO) configuration with Ir magnetic moments pointing into and out of the tetrahedral units of the pyrochlore lattice in an alternating fashion¹⁶⁻¹⁸. For compounds with the smallest R , the electrical conductivity exhibits insulating behavior even in the paramagnetic state. The phase diagram is analogous to other systems with Mott metal-insulator transitions,¹⁹ but the unusual electronic structure of $R_2\text{Ir}_2\text{O}_7$ as well as a host of anomalous thermodynamic, spectroscopic, and transport data have stimulated various proposals for topological phases and excitations³. What is missing to date is an experimental insight into the role of lattice degrees of freedom. Theoretical work (see for instance Ref.²⁰) suggests that the electron-lattice coupling plays a vital role in the determination of the ground states.

We have used polarization-resolved Raman scattering to measure the temperature evolution of phonon and magnon excitations in $R_2\text{Ir}_2\text{O}_7$ single crystals with $R = \text{Pr}$ and Eu , which together cover all phases in the diagram of Fig. 1. Whereas $\text{Pr}_2\text{Ir}_2\text{O}_7$ is a paramagnetic metal at all temperatures¹⁵, $\text{Eu}_2\text{Ir}_2\text{O}_7$ is insulating already in the paramagnetic state and exhibits AIAO order below $T_N = 115\text{ K}$.⁶ However, details of the crystal structure and magnetic ordering pattern are still under investigation^{21,22}. Since lattice distortions can relieve magnetic frustration, coupling between the spin and lattice degrees of freedom has been the subject of intense investigation for many geometrically frustrated magnets, including especially pyrochlore materials.²³⁻²⁷ The line-shapes of phonons and their renormalization at the onset of magnetic order yields specific information on the spin-

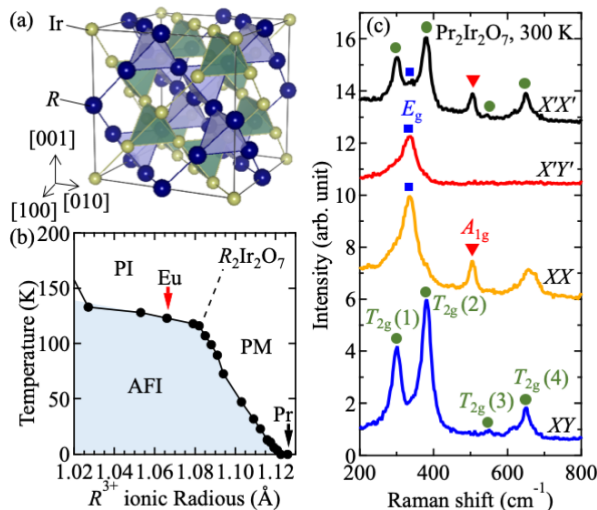


FIG. 1. (color online) (a) Schematic of the $R_2\text{Ir}_2\text{O}_7$ unit cell. The blue spheres indicate the rare-earth ions and the green ones are the iridium ions. The oxygen ions are not depicted for simplicity. (b) Phase diagram of $R_2\text{Ir}_2\text{O}_7$ as a function of rare-earth ionic radius and temperature. PI stands for paramagnetic insulator, PM stands for paramagnetic metal, and AFI stands for antiferromagnetic insulator. The $R = \text{Eu}$ and $R = \text{Pr}$ compounds are marked by arrows. (c) Raman scattering spectra of $\text{Pr}_2\text{Ir}_2\text{O}_7$ for the polarization configurations $z(\text{XX})\bar{z}$, $z(\text{XY})\bar{z}$, $z(\text{X}'\text{X}')\bar{z}$, and $z(\text{X}'\text{Y}')\bar{z}$ at room temperature. The red triangle indicates the A_{1g} mode, the blue squares are the E_g mode, and the green circles indicate the T_{2g} modes.

77 phonon coupling, and on the coupling between phonons
 78 and charge fluctuations in the case of electrically con-
 79 ducting systems. We indeed find large phonon anom-
 80 alies induced by the onset of magnetic order in $\text{Eu}_2\text{Ir}_2\text{O}_7$,
 81 and discuss them in terms of different electron-phonon
 82 coupling mechanisms. In addition, the observed Raman
 83 features are likely attributable to magnon excitations in
 84 the AIAO state, which are consistent with recent obser-
 85 vations by resonant inelastic x-ray scattering (RIXS).²⁹

86 High-quality single crystals of $\text{Pr}_2\text{Ir}_2\text{O}_7$ and $\text{Eu}_2\text{Ir}_2\text{O}_7$
 87 were grown by the KF flux method, as described
 88 previously.³⁰ In the as-grown state, the crystals are
 89 octahedron-shaped with (111) facets. We polished a
 90 (001) plane of the samples with lapping films of suffi-
 91 ciently fine grain-size for a contamination-free polariza-
 92 tion analysis. The Raman experiments were carried out
 93 with a Jobin-Yvon LabRam HR800 spectrometer using
 94 the 632.8 nm excitation line of a He-Ne laser. Laser heat-
 95 ing was minimized by keeping the laser power below 1.2
 96 mW, and all measured spectra were corrected for heat-
 97 ing following Ref. 31. Specifically, systematic measure-

98 ments of the laser power dependence of phonon energies
 99 showed that the heating is no longer negligible above 0.7
 100 mW. The laser power used in the present study may heat
 101 the sample by ~ 20 K. As we will show later, the cor-
 102 rected critical temperature, at which the spectra change
 103 markedly, is consistent with the magnetic transition tem-
 104 perature.

105 The samples were placed in a He-flow cryostat, and
 106 the measurements were conducted in backscattering ge-
 107 ometry with light propagating along the crystalline [001]
 108 axis, while the polarization of the incident and scattered
 109 light was varied within the (001) plane. The spectra were
 110 measured in four polarization configurations, namely
 111 $z(\text{XX})\bar{z}$, $z(\text{XY})\bar{z}$, $z(\text{X}'\text{X}')\bar{z}$, and $z(\text{X}'\text{Y}')\bar{z}$, where z (\bar{z})
 112 denotes the propagation direction of the incident (scat-
 113 tered) light. X (Y) represents the polarization of incident
 114 or scattered light along the [100] ([010]) crystallographic
 115 direction, and $X' = X + Y$, $Y' = X - Y$. According to
 116 a group-theoretical analysis of the pyrochlore structure
 117 (space group $Fd\bar{3}m$), the corresponding Raman spectra
 118 for the four polarization configurations are composed of
 119 $A_{1g} + E_g$, T_{2g} , $A_{1g} + E_g + T_{2g}$, and E_g contribu-
 120 tions, respectively. The unit cell of $R_2\text{Ir}_2\text{O}_7$ consists of eight
 121 formula units. The factor group analysis yields the fol-
 122 lowing optical/acoustic phonon modes^{32,33}:

$$\begin{aligned}\Gamma^{\text{op}} &= A_{1g} + E_g + 4T_{2g} \\ &\quad + 7T_{1u}. \\ \Gamma^{\text{ac}} &= T_{1u}.\end{aligned}$$

123 The first six optical modes are Raman-active, and the
 124 last seven are infrared-active.

125 Figure 1(c) shows polarization-resolved Raman spec-
 126 tra of the $R = \text{Pr}$ compound at room temperature. In
 127 the $z(\text{X}'\text{X}')\bar{z}$ geometry, in which all Raman-active lattice
 128 vibration modes are allowed, we indeed observe the six
 129 peaks expected in the $Fd\bar{3}m$ symmetry. In the $z(\text{X}'\text{Y}')\bar{z}$
 130 geometry, the expected E_g mode is clearly visible around
 131 330 cm^{-1} . In the $z(\text{XX})\bar{z}$ geometry, which allows an
 132 A_{1g} mode in addition to the E_g mode, a sharp peak is ob-
 133 served at 508 cm^{-1} and can be assigned to the A_{1g} mode.
 134 Finally, four T_{2g} peaks are observed in the $z(\text{XY})\bar{z}$ scat-
 135 tering geometry at 302 , 378 , 554 , and 646 cm^{-1} (here-
 136 after referred to as T_{2g} (1), (2), (3), and (4), respectively),
 137 in agreement with the group theoretical analysis. These
 138 modes are closely similar to phonon modes previously re-
 139 vealed in Raman experiments on isostructural pyrochlore
 140 oxides^{33,34}. The peak observed at 610 cm^{-1} in $z(\text{XY})\bar{z}$
 141 configuration and the broad one at 650 cm^{-1} in $z(\text{XX})\bar{z}$
 142 geometry can be attributed to multi-phonon modes.

143 To associate the observed modes with specific vi-
 144 bration patterns, we calculated the energy of zone-
 145 center phonon modes by density functional perturbation
 146 theory³⁵ as implemented in the Quantum ESPRESSO³⁶
 147 package, with the lattice parameters reported in Ref.
 148 30. The calculations were performed within the general-
 149 ized gradient approximation of Perdew, Burke and Ern-
 150 erhof (PBE GGA)³⁷ using the fully-relativistic ONCV

TABLE I. Observed and calculated Raman-active phonon frequencies in $R_2\text{Ir}_2\text{O}_7$ at room temperature

Material	observed/calculated frequencies (cm^{-1})					
	$T_{2g}(1)$	E_g	$T_{2g}(2)$	A_{1g}	$T_{2g}(3)$	$T_{2g}(4)$
$\text{Pr}_2\text{Ir}_2\text{O}_7$	301.8/300.0	333.3/355.5	377.9/400.9	506.0/514.2	554.3/567.1	646.2/635.3
$\text{Eu}_2\text{Ir}_2\text{O}_7$	302.5/317.4	336.8/371.2	379.5/416.9	507.8/529.6	543.1/588.0	680.2/676.8

TABLE II. Observed and calculated infrared-active phonon frequencies in $R_2\text{Ir}_2\text{O}_7$ at room temperature. The experimental data were taken from Ref.⁶.

Material	observed/calculated T_{1u} frequencies (cm^{-1})						
	$\text{Pr}_2\text{Ir}_2\text{O}_7$	105.1/107.0	149.5/149.3	203.5/208.0	339.4/354.0	412.7/438.4	464.8/481.2
$\text{Eu}_2\text{Ir}_2\text{O}_7$	114.6/112.0	149.5/150.2	206.4/220.5	339.4/367.2	433.9/461.2	487.9/497.0	633.5/625.9

151 pseudopotentials³⁸. The calculations included the spin-
 152 orbit interaction while the spin-polarization was not al-
 153 lowed. Hence the calculated systems are metallic. We
 154 used a $4 \times 4 \times 4$ k -point grid for the Brillouin-zone in-
 155 tegration and a plane-wave cutoff of 75 Ry. The results
 156 show that the A_{1g} and E_g modes are mostly composed
 157 of Ir-O bond bending modes. The T_{2g} peak with the
 158 highest frequency corresponds to Ir-O stretching modes,
 159 while the lowest two involve R-O stretching modes. The
 160 $T_{2g}(3)$ mode corresponds to vibrations of the O' ions sur-
 161 rounded by eight R ions. We show the observed and
 162 calculated Raman-active phonon frequencies for $R = \text{Pr}$
 163 and Eu in Table 1, and the infrared-active ones in Table
 164 2 with experimental data taken from Ref.⁶. Most of the
 165 peak energies are almost identical in the two compounds,
 166 except for the high-energy Ir-O stretching vibration with
 167 T_{2g} symmetry. The calculated and observed Raman ener-
 168 gies are in good agreement, except for the R-ion depen-
 169 dence which is overestimated in the calculations. This
 170 discrepancy may in part be attributable to coupling be-
 171 tween phonons and low-energy excitations of the valence
 172 electrons, which is not included here. It is noteworthy
 173 that the E_g vibration mode is two-times broader than
 174 the other modes, as previously reported for the spinel
 175 chromite CdCr_2O_4 which exhibits a strong magnetoelas-
 176 tic coupling²⁸. The same behavior is also observed for
 177 $R = \text{Eu}$ (Fig. 2), despite the different ground states of
 178 both compounds.

179 We now turn to the temperature dependence of the
 180 Raman spectra for $R = \text{Pr}$ and Eu (Fig. 2). Most
 181 of the phonon modes gradually sharpen with decreas-
 182 ing temperature, as expected as a consequence of lattice
 183 anharmonicity^{39,40}. For $\text{Pr}_2\text{Ir}_2\text{O}_7$ we note a weak addi-
 184 tional mode that appears at 450 cm^{-1} (marked by a blue
 185 triangle in Fig. 2(a)) at low temperature. Prior Raman
 186 and neutron scattering work on Pr pyrochlore compounds
 187 including $\text{Pr}_2\text{Zr}_2\text{O}_7$,⁴¹ $\text{Pr}_2\text{Ru}_2\text{O}_7$ ⁴² and $\text{Pr}_2\text{Sn}_2\text{O}_7$ ⁴³ also
 188 detected a mode at this energy, which was attributed
 189 to Pr crystal-field excitations. The strongly reduced in-
 190 tensity of this mode at elevated temperatures may then
 191 reflect scattering of conduction electrons from the local-

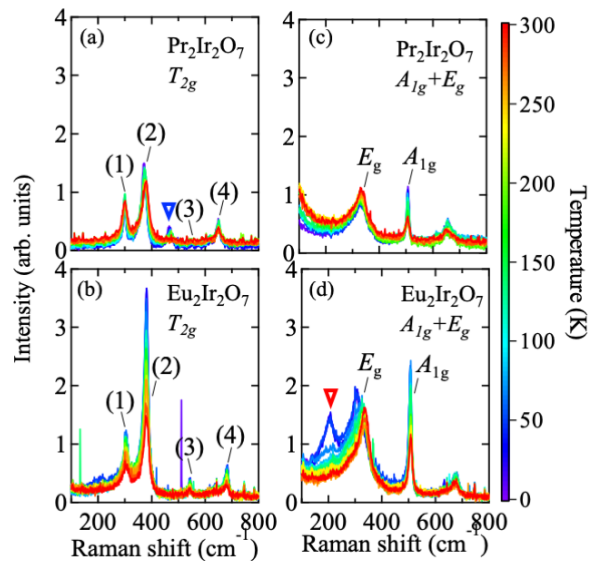


FIG. 2. (color online). Raman spectra of (a, b) T_{2g} modes and (c, d) $A_{1g} + E_g$ modes for (a, c) $R = \text{Pr}$ and (b, d) $R = \text{Eu}$ at several temperatures. The color bar represents the sample temperature.

192 ized Pr $4f$ electrons, as observed in other lanthanide
 193 compounds⁴⁴. Additional Pr crystal-field excitations are
 194 expected at lower energies ($\sim 135 \text{ cm}^{-1}$), but these exci-
 195 tations are masked in our metallic compound by intense
 196 quasielastic scattering from low-energy charge excitations
 197 of conduction electrons (Fig. 2(c)).

198 The Raman spectra of the $R = \text{Eu}$ compound exhibit
 199 a more pronounced temperature dependence (Fig. 2(d)).
 200 Upon cooling, an intense peak emerges in the E_g chan-
 201 nel around 210 cm^{-1} (marked by a red triangle), and
 202 the E_g vibration mode at higher energy shows a strong
 203 anomaly. To gain more insight into this behavior, we con-

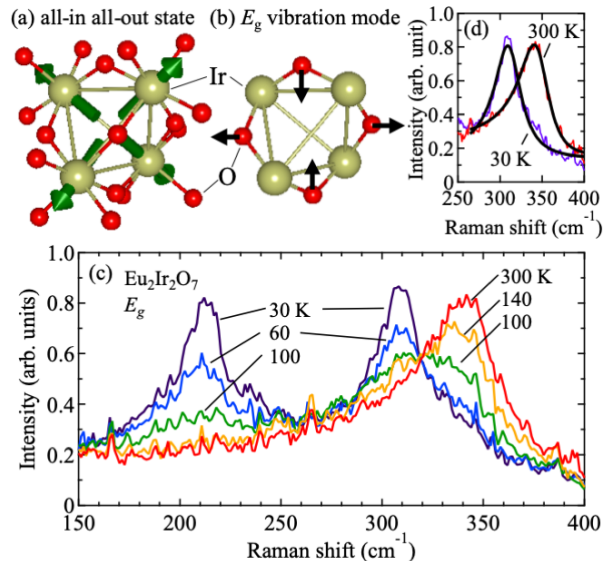


FIG. 3. (color online). (a) Schematic of the all-in/all-out magnetic ordering configuration. The arrows stand for the Ir magnetic moments. (b) Atomic displacements of the E_g lattice vibration mode. The arrows indicate the motion of the O ions. (c) Raman spectra in the $z(X'Y')z$ scattering geometry for the $R = \text{Eu}$ compound at several temperatures. (d) Raman spectra in the $z(X'Y')z$ at 30 K (purple) and 300 K (red), respectively. The fitting curves are indicated by black curves.

204 ducted more detailed measurements of the temperature
 205 dependence of the $R = \text{Eu}$ phonons in the $z(X'Y')z$ con-
 206 figuration, which only allows E_g symmetric excitations.
 207 Figure 3 displays the Raman spectra of $\text{Eu}_2\text{Ir}_2\text{O}_7$ in the
 208 energy range from 150 to 400 cm^{-1} . The new mode ap-
 209 pears upon cooling below $T \sim T_N$ and hardens from 207
 210 cm^{-1} at 100 K to 211 cm^{-1} at 30 K, while the intensity
 211 increases in a manner consistent with the magnetic order
 212 parameter. We note that earlier work on $\text{Eu}_2\text{Ir}_2\text{O}_7$ poly-
 213 crystals also reported the appearance of three new peaks
 214 below T_N ⁴⁵. The frequency of one of these peaks is close
 215 to the one we observe in E_g geometry.

216 Following the discussion for $R = \text{Pr}$ above, one might
 217 at first be tempted to assign the new peak to a Eu crystal-
 218 field excitation, although its intensity is much larger than
 219 the 450 cm^{-1} mode in $\text{Pr}_2\text{Ir}_2\text{O}_7$. However, prior work on
 220 other Eu pyrochlore compounds has shown that the Eu^{3+}
 221 ions are in a singlet ground state, and that crystal-field
 222 excitations appear only at much higher energies.⁴⁶

223 Alternatively, the 210 cm^{-1} excitation could be viewed
 224 as originating from the E_g phonon at 340 cm^{-1} . In
 225 this scenario, the double degeneracy of this mode in the
 226 paramagnetic state is split at a structural transition co-
 227 inciding with T_N , resulting in two non-degenerate E_g
 228 phonons at 210 and 310 cm^{-1} . However, the energy

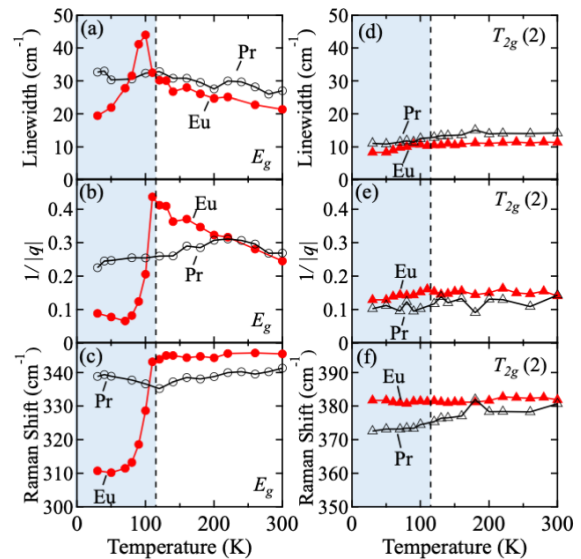


FIG. 4. (color online). Temperature dependence of (a),(d) line width, (b),(e) the inverse of the Fano asymmetry parameter $1/|q|$, and (c),(f) Raman shift of selected phonons in $\text{Eu}_2\text{Ir}_2\text{O}_7$ and $\text{Pr}_2\text{Ir}_2\text{O}_7$. Panels (a)-(c) are for the $T_{2g}(2)$ phonon mode, and (d)-(f) for the E_g mode, respectively.

229 difference between these two phonons would be about
 230 two orders of magnitude larger than typical effects of
 231 this kind in other compounds^{24–26,28}. This would imply
 232 a massive rearrangement of the lattice structure, which
 233 should also greatly affect other phonon modes and should
 234 have been detected by diffraction probes. Since such
 235 effects have not been reported, this interpretation ap-
 236 pears implausible. Based on its appearance below T_N ,
 237 we tentatively assign this mode to a single-magnon ex-
 238 citation that becomes Raman-active by virtue of the
 239 strong SOC and consequent non-coplanar magnetic order-
 240 ing pattern. The intensity of the mode is higher than
 241 in typical collinear antiferromagnets,⁴⁷ but comparable
 242 to the one for magnons in other non-collinear magnets
 243 such as the canted antiferromagnets FeBr_2 ⁴⁸ and FeF_2 ⁴⁹.
 244 The energy of the mode for $T \ll T_N$ is consistent with
 245 the zone-center gap of dispersive magnons recently re-
 246 ported by resonant inelastic x-ray scattering (RIXS).²⁹
 247 We note that, close to T_N , the RIXS data suggest a some-
 248 what stronger softening of the magnon than our Raman
 249 data. Future developments of spectroscopic techniques
 250 will serve to test our interpretation.

251 We now turn to the polarization dependence of the 210
 252 cm^{-1} mode. According to the standard Fleury-Loudon
 253 theory⁵⁰, the single-magnon excitations should appear in
 254 XY polarization (T_{2g} geometry in our notation). Indeed
 255 there is a small increase in spectral weight in this geom-
 256 etry below T_N (Fig. 2b), but the intensity in E_g geom-
 257 etry is much more pronounced (Fig. 2d). We note, how-

ever, that the Raman selection rules for magnetic excitations in non-collinear structures can be quite complex, as documented for instance in experimental and theoretical work on the magnetic field-induced canted state in La_2CuO_4 ^{51,52} which revealed magnon modes that are forbidden in the Fleury-Loudon theory. In addition, longitudinal magnetic excitations with selection rules different from those of the standard transverse magnons have recently been found in Raman experiments on Ca_2RuO_4 , a material that (like $\text{Eu}_2\text{Ir}_2\text{O}_7$) exhibits a metal-insulator transition and comprises soft pseudospins composed of both spin and orbital components⁵³. Finally, there is still considerable uncertainty regarding details of the magnetic ground state, which can also influence the Raman selection rules^{21,22}. To conclusively establish the origin of the 210 cm^{-1} mode, further investigations of the magnetic ground state and the Raman selection rules of low-energy magnetic excitations are therefore required.

In view of the asymmetric lineshape of the observed phonons, we fitted them with Fano profiles written as $I(\omega) = I_0(q + \epsilon)^2 / (1 + \epsilon^2)$, where $\epsilon = (\omega - \omega_0) / \Gamma$, ω_0 is the resonant energy, Γ is the linewidth of the vibrational state, and q is the Fano asymmetry parameter⁵⁴ which measures the ratio of phonon scattering to the background scattering amplitude yielded by an excitation continuum. The E_g spectra at all temperatures are well fitted with Fano profiles, as demonstrated in Fig. 3(d). Figure 4 displays the temperature dependence of the resulting fitting parameters. Whereas the parameters characterizing the phonons in $\text{Pr}_2\text{Ir}_2\text{O}_7$ and the T_{2g} modes in $\text{Eu}_2\text{Ir}_2\text{O}_7$ exhibit smooth temperature dependences without any discernible anomalies (Fig. 4(d)-(f)), the E_g lattice vibration mode in $\text{Eu}_2\text{Ir}_2\text{O}_7$ is highly anomalous (Fig. 4(a)-(c)). The phonon energy is nearly temperature independent in the paramagnetic state, but abruptly decreases by $\sim 35\text{ cm}^{-1}$ below T_N . In contrast to the other phonons, the linewidth of the E_g mode increases with decreasing temperature in the paramagnetic state, and exhibits a sharp maximum below T_N while the Fano asymmetry $1/|q|$ drops by a factor of four.⁵⁵

We first address the large softening of the E_g phonon. Phonon energy shifts can in principle be caused by modulations of the static lattice structure across the magnetic transition. Since the specific heat indicates that the transition is continuous⁴, the modulated lattice structure should be described by a subgroup of $Fd\bar{3}m$. Continuous structural transitions have indeed been observed in other geometrically frustrated magnets with $Fd\bar{3}m$ symmetry, including pyrochlore-type $\text{Cd}_2\text{Re}_2\text{O}_7$ ^{24,25} and spinel-type $(\text{Cd,Zn})\text{Cr}_2\text{X}_4$ ($X=\text{O}, \text{S}, \text{Se}$)²⁶⁻²⁸. In each case, phonon peak splittings were reported not only for the E_g symmetry, but also for modes in other scattering geometries, in contrast to our data. Furthermore, previous x-ray and neutron diffraction studies of $\text{Eu}_2\text{Ir}_2\text{O}_7$ and other pyrochlore iridates report no indication of a lowering of the lattice symmetry^{16,18,56}.

Frequency shifts of optical modes can also occur as a consequence of magnetostrictive effects following the

Grüneisen law, as observed for instance in multiferroic RCrO_3 which shows an abrupt lattice volume modification below the magnetic transition temperature^{57,58}. In the case of $\text{Eu}_2\text{Ir}_2\text{O}_7$, however, there is almost no anomaly in the temperature dependence of the lattice constants⁵⁶. Finally, we note that Liang *et al.* discovered a C_4 symmetry breaking in the $R = \text{Eu}$ compound by using torque magnetometry²¹, which was later attributed to multipolar ordering²². The present Raman spectra may be more sensitive to subtle structural distortions associated with electronic ordering phenomena than standard x-ray experiments.

Nonetheless, the large shift of the E_g phonon energy at T_N is difficult to explain on the basis of static atomic displacements alone. This conclusion is underscored by the observation of the pronounced Fano lineshape of this mode, which indicates dynamical coupling of the vibrational mode to a continuum of excitations, and by the large anomalies of the parameters Γ and $1/|q|$ at T_N . We distinguish three different mechanisms that can lead to such anomalies:

(i) Modulation of the exchange interactions via excitation of phonons. This spin-phonon coupling mechanism^{59,60} has been widely discussed for insulating compounds with $3d$ valence electrons^{28,61-65}. Recently, an extended model, which includes spin-space anisotropies, has been shown to account for the energy shift of phonons in $\text{Cd}_2\text{Os}_2\text{O}_7$ ⁶⁶ (where phonon anomalies of magnitude comparable to those in $\text{Eu}_2\text{Ir}_2\text{O}_7$ have been reported). The linewidth anomalies at the magnetic ordering transition generated by this mechanism are rather small in conventional magnetic insulators, but can become substantial if there are pronounced intersite spin-orbital fluctuations in the paramagnetic state,⁶⁷ which may well be the case in $\text{Eu}_2\text{Ir}_2\text{O}_7$. We also note that the E_g mode corresponds to an Ir-O-Ir bending mode (Fig. 3b), which is expected to modulate the superexchange interaction or Dzyaloshinskii-Moriya interaction between Ir pseudospins. These interactions can play an important role in the stabilization of the all-in all-out magnetic order, as suggested in Ref.⁶⁸. It should be noted that the A_{1g} mode, which is also an Ir-O-Ir bending mode with the same phase, shows no observable energy shift below T_N . This may indicate deviations of the magnetic ordering pattern from the perfect all-in all-out state, as suggested in Ref.¹³ and²².

(ii) Phonon-induced modulation of the orbitals, which affects magnetism via the on-site spin-orbit coupling. This mechanism has been discussed for the insulating square-lattice iridates^{31,69}. In iridates with the orbitally non-degenerate $J = \frac{1}{2}$ ground state, including $\text{Eu}_2\text{Ir}_2\text{O}_7$, dynamical admixture of the $J = \frac{3}{2}$ levels can generate substantial pseudospin-phonon coupling and phonon linewidth anomalies.

(iii) Electron-phonon coupling through charge fluctuations. This effect can lead to large phonon lineshape anomalies at spin density wave transitions in metals which open up gaps on the Fermi surface, as observed

for instance in the iron pnictides⁷⁰. $\text{Eu}_2\text{Ir}_2\text{O}_7$ exhibits an optical gap of ~ 200 meV, much larger than the phonon energy, but the gap is soft and shows a long low-energy tail.⁶ The electrical conductivity of $\text{Eu}_2\text{Ir}_2\text{O}_7$ decreases with decreasing temperature, but its magnitude is substantial in the paramagnetic state and decreases sharply upon cooling below T_N . Temperature dependent charge fluctuations may therefore also contribute to the phonon anomalies in this material.

These considerations suggest that the Ir-O-Ir bond-bending vibration in $\text{Eu}_2\text{Ir}_2\text{O}_7$ is strongly coupled to a continuum composed of spin, charge, and orbital excitations via a confluence of all three mechanisms. The increase of the Fano asymmetry upon cooling in the paramagnetic state (Fig. 4c) may reflect an extended critical fluctuation regime, which is expected in view of the geometrically frustrated pyrochlore structure. With the onset of all-in/all-out magnetic order, a gap (or pseudogap) of magnitude larger than the phonon energy develops in this continuum, so that the coupling is quenched and the Fano asymmetry is reduced (Fig. 4(b)). Since electronic spectral weight is expected to pile up at energies above the gap, the non-monotonic T -dependence of the linewidth Γ may be a consequence of the continuous closure of the gap upon approaching T_N . An analogous temperature evolution of Γ is also observed for some phonons

in high-temperature superconductors due to the opening of the superconducting gap.⁷¹

In conclusion, our Raman experiments on $\text{Eu}_2\text{Ir}_2\text{O}_7$ have revealed unusually strong anomalies of a specific phonon mode that involves Ir-O-Ir bond bending vibrations. These data should motivate in-depth theoretical work on the microscopic mechanism responsible for the electron-phonon coupling, and on the influence of electron-phonon interactions on the anomalous electronic properties and phase behavior of the pyrochlore iridates and related compounds.

We are grateful to Hakuto Suzuki and Giniyat Khalullin for fruitful discussions. This work was supported by the Deutsche Forschungsgemeinschaft (DFG, German Research Foundation) - Projektnummer 107745057 - TRR 80, by the Japan Society for the Promotion of Science through the Funding Program for World-Leading Innovative R&D on Science and Technology (FIRST Program) on 'Quantum Science on Strong Correlation' initiated by the Council for Science and Technology Policy, by JSPS Grant-in-Aid for Scientific Research (No. 26103006, No. 24224009, 18H04214, and 16H00981), and by PRESTO (No. JPMJPR15R5) and CREST (No. JPMJCR16F1 and JPMJCR1874), Japan Science and Technology Japan.

-
- ¹ B. Keimer and J.E. Moore, *Nat. Phys.* **13**, 1045 (2017).
² B. J. Kim *et al.*, *Phys. Rev. Lett.* **101**, 076402 (2008).
³ W. Witczak-Krempa, G. Chen, Y.B. Kim, L. Balents, *Annu. Rev. Condens. G.* **5**, 57 (2014).
⁴ K. Matsuhira, M. Wakeshima, Y. Hinatsu, and S. Takagi, *J. Phys. Soc. Jpn.* **80**, 094701 (2011).
⁵ K. Ueda *et al.*, *Phys. Rev. Lett.* **109**, 136402 (2012).
⁶ K. Ueda, J. Fujioka, and Y. Tokura, *Phys. Rev. B* **93**, 245120 (2016).
⁷ M. Sakata *et al.*, *Phys. Rev. B* **83**, 041102 (2011).
⁸ F. F. Tafti, J. J. Ishikawa, A. McCollam, S. Nakatsuji, and S. R. Julian, *Phys. Rev. B* **85**, 205104 (2012).
⁹ K. Ueda, J. Fujioka, C. Terakura, and Y. Tokura, *Phys. Rev. B* **92**, 121110 (2015).
¹⁰ K. Ueda, J. Fujioka, B.-J. Yang, J. Shiogai, A. Tsukazaki, S. Nakamura, S. Awaji, N. Nagaosa, and Y. Tokura, *Phys. Rev. Lett.* **115**, 056402 (2015).
¹¹ Z. Tian *et al.*, *Nat. Phys.* **12**, 134 (2016).
¹² K. Ueda, T. Oh, B.-J. Yang, R. Kaneko, J. Fujioka, N. Nagaosa, and Y. Tokura, *Nat. Commun.* **8**, 15515 (2017).
¹³ K. Ueda, R. Kaneko, H. Ishizuka, J. Fujioka, N. Nagaosa, and Y. Tokura, *Nat. Commun.* **9**, 3032 (2018).
¹⁴ S. Nakatsuji, Y. Machida, Y. Maeno, T. Tayama, T. Sakakibara, J. van Duijn, L. Balicas, J. N. Millican, R. T. Macaluso, and Julia Y. Chan, *Phys. Rev. Lett.* **96**, 087204 (2006).
¹⁵ T. Kondo *et al.*, *Nat. Commun.* **6**, 10042 (2015).
¹⁶ H. Sagayama, D. Uematsu, T. Arima, K. Sugimoto, J. J. Ishikawa, E. O'Farrell, and S. Nakatsuji, *Phys. Rev. B* **87**, 100403 (2013).
¹⁷ K. Tomiyasu, K. Matsuhira, K. Iwasa, M. Watahiki, S. Takagi, M. Wakeshima, Y. Hinatsu, M. Yokoyama, K. Ohoyama, and K. Yamada, *J. Phys. Soc. Jpn.* **81**, 034709 (2012).
¹⁸ H. Guo, C. Ritter, and A. C. Komarek, *Phys. Rev. B* **94**, 161102(R) (2016).
¹⁹ M. Imada, A. Fujimori, and Y. Tokura, *Rev. Mod. Phys.* **70**, 1039 (1998).
²⁰ B.-J. Yang and Y. B. Kim, *Phys. Rev. B* **82**, 085111 (2010).
²¹ T. Liang, T. H. Hsieh, J. J. Ishikawa, S. Nakatsuji, L. Fu, and N. P. Ong, *Nature Phys.* **10**, 1038 (2017).
²² Y. Wang, H. Weng, L. Fu, and X. Dai, *Phys. Rev. Lett.* **119**, 187203 (2017).
²³ J. S. Gardner, M. J. P. Gingras, and J. E. Greedan, *Rev. Mod. Phys.* **82**, 53 (2010).
²⁴ C. S. Knee *et al.*, *Phys. Rev. B* **71**, 214518 (2005).
²⁵ J.-I. Yamaura, K. Takeda, Y. Ikeda, N. Hirao, Y. Ohishi, T. C. Kobayashi, and Z. Hiroi, *Phys. Rev. B* **95**, 020102 (2017).
²⁶ A. B. Sushkov, O. Tchernyshyov, W. Rattliff II, S. W. Cheong, and H. D. Drew, *Phys. Rev. Lett.* **94**, 137202 (2005).
²⁷ V. Gnezdilov, P. Lemmens, Y. G. Pashkevich, Ch. Payen, K. Y. Choi, J. Hemberger, A. Loidl, and V. Tsurkan, *Phys. Rev. B* **84**, 045106 (2011).
²⁸ Ch. Kant *et al.*, *Phys. Rev. B* **80**, 214417 (2009).
²⁹ S. H. Chun *et al.*, *Phys. Rev. Lett.* **120**, 177203 (2018).
³⁰ J. N. Millican *et al.*, *Mater. Res. Bull.* **42**, 928 (2007).
³¹ H. Gretarsson, N. H. Sung, M. Höppner, B. J. Kim, B. Keimer, and M. Le Tacon, *Phys. Rev. Lett.* **116**, 136401 (2016).
³² H. C. Gupta, S. Brown, N. Rani, and V. B. Gohel, *J.*

- 487 Raman Spectrosc. **32**, 41 (2001).
488 ³³ M. T. Vandenborre, E. Husson, J. P. Chatry, and D.
489 Michel, J. Raman Spectrosc. **14**, 63 (1983).
490 ³⁴ K. Taniguchi, T. Katsufuji, S. Iguchi, Y. Taguchi, H. Tak-
491 agi, and Y. Tokura, Phys. Rev. B **70**, 100401 (2004).
492 ³⁵ S. Baroni, S. de Gironcoli, A. Dal Corso, and P. Giannozzi,
493 Rev. Mod. Phys. **73**, 515 (2001).
494 ³⁶ P. Giannozzi, S. Baroni, N. Bonini, M. Calandra, R. Car,
495 C. Cavazzoni, D. Ceresoli, G. L. Chiarotti, M. Cococcioni,
496 I. Dabo *et al.*, J. Phys.: Condens. Matter **21**, 395502
497 (2009).
498 ³⁷ J. P. Perdew, K. Burke, and M. Ernzerhof, Phys. Rev.
499 Lett. **77**, 3865 (1996).
500 ³⁸ P. Scherpelz, M. Govoni, I. Hamada, G. Galli, J. Chem.
501 Theory Comput. **12**, 3523 (2016).
502 ³⁹ P. G. Klemens, Phys. Rev. **148**, 845 (1966).
503 ⁴⁰ M. Balkanski, R. F. Wallis, and E. Haro, Phys. Rev. B **28**,
504 1928 (1983).
505 ⁴¹ K. Kimura, S. Nakatsuji, J.-J. Wen, C. Broholm, M.B.
506 Stone, E. Nishibori, and H. Sawa, Nat. Comm. **4**, 1934
507 (2013).
508 ⁴² J. van Duijn *et al.*, Phys. Rev. B **96**, 094409 (2017).
509 ⁴³ S. Saha, S. Prusty, S. Singh, R. Suryanarayanan, A.
510 Revcolevschi, and A.K. Sood, J. Sol. State Chem. **184**,
511 2204 (2011).
512 ⁴⁴ R. Feile, M. Loewenhaupt, J. K. Kjems, and H. E. Hoenig,
513 Phys. Rev. Lett. **47**, 610 (1988).
514 ⁴⁵ T. Hasegawa, N. Ogita, K. Matsuhira, S. Takagi, M.
515 Wakeshima, Y. Hinatsu, and M. Udagawa, J. Phys.: Conf.
516 Ser. **200**, 012054 (2010).
517 ⁴⁶ A. Nag, P. Dasgupta, Y.M. Jana, and D. Ghosh, J. Alloy
518 Compd. **384**, 6 (2004).
519 ⁴⁷ W. Hayes and R. Loudon, *Scattering of light by crystals*
520 (Dover Publications Inc., Mineola, New York).
521 ⁴⁸ G. C. Psaltakis, G. Mischler, D. J. Lockwood, M. G. Cot-
522 tam, A. Zwick, and S. Legrand, J. Phys. C **17**, 1735 (1984).
523 ⁴⁹ D. J. Lockwood, M. G. Cottam, V. C. Y. So, and R. S.
524 Katiyar, J. Phys. C: Solid State Phys. **17**, 6009 (1984).
525 ⁵⁰ P. A. Fleury and R. Loudon, Phys. Rev. **166**, 514 (1968).
526 ⁵¹ M. B. Silva Neto and L. Benfatto, Phys. Rev. B **72**,
527 140401(R) (2005).
528 ⁵² L. Benfatto, M. B. Silva Neto, A. Gozar, B. S. Dennis, G.
529 Blumberg, L. L. Miller, Seiki Komiyama, and Yoichi Ando,
530 Phys. Rev. B **74**, 024416 (2006).
531 ⁵³ S.-M. Souliou *et al.*, Phys. Rev. B **119**, 067201 (2017).
532 ⁵⁴ U. Fano, Phys. Rev. **124**, 1866 (1961).
533 ⁵⁵ We note that the integrated spectral weights of the 310
534 cm^{-1} feature below T_N and the 340 cm^{-1} feature above T_N
535 are identical within the experimental error, after account-
536 ing for the thermal occupation factor. We also note that
537 these data can be fitted by a superposition of two profiles
538 with T -independent frequencies and T -dependent spec-
539 tral weight, rather than a single profile with T -dependent
540 frequency and spectral weight. This scenario would imply
541 a (perhaps weakly) first-order magnetic or magneto-
542 structural transition that was not reported in prior work
543 on this compound, but cannot be completely ruled out
544 based on the data at hand.
545 ⁵⁶ H. Takatsu, K. Watanabe, K. Goto, and H. Kadowaki,
546 Phys. Rev. B **90**, 235110 (2014).
547 ⁵⁷ M. Udagawa, K. Kohn, N. Kashizuka, and T. Tsushima,
548 Solid State Commun. **16**, 779 (1975).
549 ⁵⁸ V. S. Bhadram, B. Rajeswaran, A. Sundaresan, and C.
550 Narayana, EPL **101**, 17008 (2013).
551 ⁵⁹ W. Baltensperger, J. Appl. Phys. **41**, 1052 (1970).
552 ⁶⁰ N. Suzuki and H. Kamimura, J. Phys. Soc. Jpn. **35**, 985
553 (1973).
554 ⁶¹ D. J. Lockwood and M. G. Cottam, J. Appl. Phys. **64**,
555 5876 (1988).
556 ⁶² K. Wakamura and T. Arai, J. Appl. Phys. **63**, 5824 (1988).
557 ⁶³ E. Granado, N. O. Moreno, A. Garcia, J. A. Sanjurjo, C.
558 Rettori, I. Torriani, S. B. Oseroff, J. J. Neumeier, M. J.
559 McClellan, S.-W. Cheong, and Y. Tokura, Phys. Rev. B
560 **58**, 11435 (1998).
561 ⁶⁴ E. Granado *et al.*, Phys. Rev. B **60**, 11879 (1999).
562 ⁶⁵ J. Laverdière *et al.*, Phys. Rev. B **73**, 214301 (2006).
563 ⁶⁶ C. H. Sohn *et al.*, Phys. Rev. Lett. **118**, 117201 (2017).
564 ⁶⁷ C. Ulrich, G. Khaliullin, M. Guennou, H. Roth, T. Lorenz,
565 and B. Keimer, Phys. Rev. Lett. **115**, 156403 (2015).
566 ⁶⁸ Maged Elhajal, Benjamin Canals, Raimon Sunyer, and
567 Claudine Lacroix, Phys. Rev. B **71**, 094420 (2005).
568 ⁶⁹ H. Gretarsson, J. Saucedo, N. H. Sung, Höppner, M. Mi-
569 nola, B. J. Kim, B. Keimer, and M. Le Tacon Phys. Rev.
570 B **96**, 115138 (2017).
571 ⁷⁰ M. Rahlenbeck, G. L. Sun, D. L. Sun, C. T. Lin, B. Keimer,
572 and C. Ulrich, Phys. Rev. B **80**, 064509 (2009).
573 ⁷¹ M. Bakr, A. P. Schnyder, L. Klam, D. Manske, C. T. Lin,
574 B. Keimer, M. Cardona, and C. Ulrich, Phys. Rev. B **80**,
575 064505 (2009).